The Characteristics and Mechanisms of Uptake of PLGA Nanoparticles in Rabbit Conjunctival Epithelial Cell Layers

Mohamed G. Qaddoumi,[1] Hideo Ueda,[1] Johnny Yang,[1] Jasmine Davda,[3] Vinod Labhasetwar,[3,4] and Vincent H. L. Lee[1,2,5]

Received July 22, 2003; accepted December 14, 2003

Purpose. To delineate the characteristics and mechanisms of uptake of biodegradable poly(D,L-lactide-*co*-glycolide) (PLGA) nanoparticles in primary cultured rabbit conjunctival epithelial cells (RCECs).

Methods. Poly(D,L-lactide-*co*-glycolide) nanoparticles (PLGA 50:50, 100 nm in diameter) containing 6-coumarin (as a fluorescent marker) were used. The effect of size was studied using various particle sizes (100 nm, 800 nm, and 10 μm). The effect of cytochalasin D, nocodazole, and metabolic inhibitors on nanoparticle uptake was investigated. The capability of nanoparticles to enhance the uptake of an encapsulated protein, BSA bound to Texas red (TR-BSA), was evaluated.

Results. Maximal uptake of nanoparticles at 37°C occurred at 2 h, and 100-nm particles had the highest uptake in RCECs in comparison with 800-nm and 10-μm particles. Nanoparticle uptake was saturable over the 0.1–4 mg/ml concentration range. Nanoparticle uptake was confirmed by confocal microscopy and was inhibited significantly by coumarin-free nanoparticles (of similar size), by lower incubation temperature, and by the presence of metabolic inhibitors and cytochalasin D. The uptake of encapsulated TR-BSA in RCECs at 4 h was 28% higher than free BSA application.

Conclusion. Our findings suggest that PLGA nanoparticle uptake in primary cultured rabbit conjunctival epithelial cells occurs most likely by adsorptive-type endocytosis.

KEY WORDS: absorption; endocytosis; ocular drug delivery; ophthalmic; polymeric microparticles.

INTRODUCTION

Topical ophthalmic drugs have generally poor absorption in the eye due to the cornea's low permeability to drugs and noncorneal factors such as rapid tear turnover, nasolacrimal drainage, and systemic absorption. Most noninvasive approaches for enhancing ocular drug absorption involve the use of prodrugs, the use of viscosity agents designed to prolong the drug residence time, and colloidal systems (1). Polymeric nanoparticles are an attractive colloid because they demonstrate increased stability and have a longer elimination half-life in tear fluid, 20 min, than do conventional drugs applied topically to the eye, which have half-lives of just 1–3 min (2).

Nanoparticles have been evaluated as ocular drug delivery systems to enhance the absorption of therapeutic drugs, improve bioavailability, reduce systemic side effects, and sustain intraocular drug levels (3–6). In addition, polymeric nanoparticles have been shown to have potential in the treatment of inflammatory external eye diseases (7). PLGA is a copolymer of poly (D,L-lactide-*co*-glycolide) and is an ideal candidate of biodegradable polymers for formulation into nanoparticles due to its wide medical use, biocompatibility, and safety (8).

The conjunctival epithelium is a thin, vascular membrane lining the inside of the eyelids and has been shown to express several membrane transporters. Physiologically, it may function as a protective barrier against the permeation of pathogens and exogenous drugs, in the exchange of nutrients and solutes with the cornea, and in the excretion of solutes and endogenous enzymes contributing to tear content and function (9). The larger surface area and paracellular pore size of the conjunctival epithelium allow for higher drug permeability than is seen in the corneal epithelium (10). Drug and solute transport across the conjunctival epithelium has extensively been studied. However, the transport and absorption of nanoparticles in the conjunctival epithelium has not been considerably studied. Primary cultured rabbit conjunctival epithelial cells (RCECs) have similar permeability values to low-molecular-weight drugs as isolated rabbit conjunctiva, which suggests that RCEC culture may be useful as an *in vitro* model for evaluating drug transport (11).

In the current study, we used a primary cultured RCEC model to investigate the uptake characteristics of biodegradable PLGA nanoparticles (100 nm in diameter) and to elucidate the mechanism of their uptake. We also sought to demonstrate the capability of nanoparticles to enhance ocular absorption by studying the uptake of a model, encapsulated agent, bovine serum albumin, in RCECs.

MATERIALS AND METHODS

Materials

Nanoparticles of polylactic polyglycolic acid co-polymer (PLGA 50:50, with an inherent viscosity of 1.31 measured in hexafluoroisopropanol) with mean diameters of 100 nm, 800 nm, and 10 μm (actual diameters were 0.11 ± 0.05 μm, 0.8 ± 0.02 μm, and 9.4 ± 0.2 μm, respectively) were obtained from the coauthor Dr. Labhasetwar and formulated and characterized with the methods reported by Davda and Labhasetwar (12). The nanoparticles contained bovine serum albumin (4% w/w) as a model protein and 6-coumarin (0.05% w/w) as a fluorescent marker. In addition, his laboratory provided 100-nm unloaded PLGA nanoparticles and 100 nm PLGA nanoparticles containing 25% (w/w) bovine serum albumin (14.5%, unconjugated and 10.4% conjugated to Texas red marker). 6-coumarin was purchased from Polysciences Inc. (Warrington, PA, USA). Culture media and supplies were purchased from Invitrogen Corp. (Carlsbad, CA, USA). PC-1 serum-free culture medium was purchased from Biowhittaker (Walkersville, MD, USA). Clearwell filters (12-mm diameter,

[1] Department of Pharmaceutical Sciences, University of Southern California, Los Angeles, California 90089-9121.
[2] Department of Ophthalmology, University of Southern California, Los Angeles, California 90089-9121.
[3] Department of Pharmaceutical Sciences, University of Nebraska Medical Center, Omaha, Nebraska 69198-6025.
[4] Biochemistry and Molecular Biology, University of Nebraska Medical Center, Omaha, Nebraska 69198-6025.
[5] To whom correspondence should be addressed. (e-mail: vincentl@usc.edu)

0724-8741/04/0400-0641/0 © 2004 Plenum Publishing Corporation

0.4-μm pore size) were obtained from Costar (Cambridge, MA, USA). Nystatin, nocodazole, cytochalasin D, and Texas-red conjugated bovine serum albumin were obtained from Sigma Chemical Co. (St. Louis, MO, USA). Lucifer yellow was purchased from Molecular Probes (Eugene, OR, USA).

Animals and Tissue Preparation

Conjunctival tissue was isolated and prepared as previously described by Kompella *et al.* (13). Briefly, male Dutch-belted pigmented rabbits, weighing 2.0–2.5 kg, were obtained from Irish Farms (Norco, CA, USA) and handled in accordance with Guiding Principles in the Care and Use of Animals (DHEW Publication, NIH 80-23). The animals were euthanized with an overdose of sodium pentobarbital solution (325 mg/kg) injected via the ear marginal vein. Eyeballs were carefully excised and then the conjunctival tissues were carefully dissected.

In vitro Release of 6-Coumarin from Nanoparticles

Ten-milliliter nanoparticle suspension (1 mg/ml) prepared in bicarbonate Ringer's solution (BRS) was placed on a shaker for 24 h at 37°C. Periodic samples (1 ml) were then taken and replaced with fresh BRS buffer of equivalent volume. Each sample was then subjected to centrifugation at 10,000 × *g* for 5 min. The supernatant was collected, lyophilized overnight, extracted, and analyzed for the released 6-coumarin content, as described in "Analytical Method," below. To determine the amount of 6-coumain released from PLGA nanoparticles, we constructed a standard curve of nanoparticles (concentrations ranging from 0.1 to 500 μg/ml) in BRS with subsequent lyophilization, extraction, and analysis as done for the *in vitro* released samples.

Primary Air-Interfaced Culture of Rabbit Conjunctival Epithelial Cells

Rabbit conjunctival epithelial cells were harvested using a protocol developed by Saha *et al.* (14) and modified by Yang *et al.* (15). Briefly, following excision, the conjunctiva was washed in ice-cold Ca^{2+}/Mg^{2+}-free Hank's balanced salt solution and treated with 0.2% protease type XIV (Sigma Chemical Co.) for 60 min at 37°C in 95% air/5% CO_2 to dissociate the cells. The isolated cells were treated with Minimum Essential Medium (S-MEM) containing 10% fetal bovine serum (FBS) and 1 mg/ml deoxyribonuclease (DNAase I) to stop protease reaction. The cell pellet was washed, centrifuged at 100 × *g* for 10 min at room temperature, and then filtered through a 40-μm cell strainer. The final cell pellet was resuspended in Dulbecco's Modified Eagle Medium/Nutrient Mixture F-12 (DMEM/F12) medium supplemented with 100 U/ml penicillin–streptomycin, 0.5% gentamicin, 0.4% fungizone, 2 mM L-glutamine, 1% ITS^+ (6.5 μg/ml insulin, 6.5 μg/ml transferrin, 6.5 ng/ml selenious acid, 1.25 mg/ml BSA, and 5.35 mg/ml linoleic acid), 30 μg/ml bovine pituitary extract (BPE), 1 μM hydrocortisone, and 1 ng/ml epidermal growth factor (EGF). These cells were seeded on Clearwells precoated with rat-tail collagen at a density of 1.2×10^6 cells/cm^2 and then were cultured at 37°C in 5% CO_2 and 95% air. From day 2 onward, the growth medium was changed to PC-1 growth medium supplemented with 2 mM L-glutamine, 100 U/ml penicillin–streptomycin, 0.5% gentamicin, and 0.4% fungizone. Cells were switched to an air-interface (i.e., nominally fluid-free on the apical surface of the cell layers) on day 4 onward. On days 6 or 7, cells became confluent and were used for experiments.

Nanoparticle Uptake Study in RCECs

Following confluency of cultured conjunctival cells, the culture medium from both sides of the cells was replaced with a physiological BRS, and the cells were incubated at 37°C for 30 min. BRS consisted of 116 mM NaCl, 5.6 mM KCl, 1.8 mM $CaCl_2 \cdot 2H_2O$, 5.5 mM D-glucose, 0.8 mM NaH_2PO_4, 0.8 mM $MgCl_2$, 25 mM $NaHCO_3$, and 15 mM *N*-2-hydroxyethylpiperazine-*N*-2-ethanesulfonic acid (HEPES). Before it was used, the BRS was bubbled with air containing 5% CO_2 and adjusted to pH 7.4 before usage. The osmolarity of the solution was in the range 290–310 mOsm. All nanoparticle suspensions were prepared in BRS solution. After 30 min incubation with BRS, the apical side of conjunctival epithelial cells was replaced with the nanoparticle suspension and incubated for 0–4 h at 37°C. After incubation, the apical solution was aspirated, and the cell filters were washed three times with ice-cold BRS buffer solution to remove excess nanoparticles. The cell filters were then cut off from the Clearwells with a blade and transferred separately into covered disposable tubes with 1 ml BRS solution. For the determination of the amount of membrane-bound fraction of nanoparticles, washed cells were trypsinized with 10x Trypsin-EDTA for 30 min to a total volume of 1 ml and centrifuged twice at 1000 × *g* for 10 min each. The resulting pellet was solubilized with 0.5 ml of 0.5% Triton-X 100 in BRS for 30 min at 37°C and diluted to 1 ml with BRS. The filter samples and/or both the supernatant and dissolved pellet (1 ml each) of each sample were then frozen at −20°C and lyophilized overnight.

The effect of the nanoparticles on the bioelectric parameters of the conjunctival epithelial cell culture was examined by evaluating the change in both the transepithelial electrical resistance (TEER) and potential difference (PD) after 2 h of incubation with nanoparticles. The TEER and PD were measured using a Voltohmmeter electrode (World Precision Instruments, Sarasota, FL, USA). The cell layer resistance was obtained by subtracting the total resistance from blank filter resistance, corrected for the specific Transwell surface area, and expressed as $\Omega \cdot cm^2$. Similarly, the PD was calculated and expressed as mV.

Analytical Method

The lyophilized samples were extracted with 1 ml ethyl acetate and centrifuged three times at 1000 × *g* for 3 min each. The combined extract (total of 3 ml) was evaporated under nitrogen stream. The sample residues were then reconstituted with 400 μl acetonitrile. Samples from 6-coumarin- and Texas-red bovine serum albumin (TR-BSA)-loaded nanoparticles were analyzed with a spectrofluorometer F-2000 (Hitachi, Tokyo, Japan) set at an excitation wavelength of 450 nm and an emission wavelength of 490 nm or an excitation wavelength of 590 nm and an emission wavelength of 645 nm, respectively. Standard curves for 6-coumarin and Texas red were constructed for each nanoparticle uptake experiment by spiking different known concentrations of nanoparticles (12.5–200 μg/ml) in BRS and treating them the same way as nanoparticle samples (lyophilized and extracted as before).

The amount of nanoparticles taken up by rabbit conjunctival epithelial cells was then determined from the standard curve.

Characteristics of Nanoparticle Uptake

Effect of Incubation Time and Particle Size

To characterize the uptake mechanism of nanoparticles in RCECs, 6-coumarin–loaded nanoparticles were used for all these experiments. Various sizes of particles (100 nm, 800 nm, and 10 μm) at 0.65 mg/ml were incubated in RCECs for 2 h and the uptake was then analyzed. Time-dependent uptake study was carried out using 100-nm-size nanoparticles at 0.3 mg/ml from 0 to 4 h. The optimal time for uptake was chosen for all other experiments.

Effect of Nanoparticle Concentration, Competition, and Temperature

To investigate if nanoparticle uptake was saturable, RCECs were incubated for 2 h with nanoparticles in the concentration range of 1 to 4 mg/ml. Temperature-dependent uptake studies were carried out with three different nanoparticle concentrations (0.3, 0.5, and 1 mg/ml) at both 37°C and 4°C. The activation energy (E_a) for the temperature-dependent uptake of the three different nanoparticle concentrations was calculated using Arrhenius analysis [$E_a = (T_1T_2R / T_2 - T_1) \times \ln k_2/k_1$, where T_1 and T_2 are the temperatures in Kelvin, R is the gas constant, and k_2 and k_1 represent the uptake rate constant at each temperature]. The average activation energy is obtained by averaging the E_a at all three different nanoparticle concentrations. For the competition study, nanoparticles were incubated for 2 h at 100 μg/ml in the absence and presence of an excess amount of coumarin-free unloaded nanoparticles (5–10-fold higher concentration).

Mechanism of Nanoparticle Uptake and Drug Delivery Enhancement

To evaluate if nanoparticle uptake occurs through an active process, RCECs were preincubated with metabolic inhibitors (10 mM sodium azide and 0.2 mM 2,4-dinitrophenol) for 30 min prior to nanoparticle uptake and throughout the 2-h uptake period. The effect of microfilament and microtubule inhibitors (also known as vesicle formation or endocytosis inhibitors) on nanoparticle uptake in RCECs was evaluated by preincubating cells with 0.1 μg/ml cytochalasin D (microfilament inhibitor) and 1 μg/ml nocodazole (microtubule inhibitor) (both dissolved in DMSO), respectively, for 30 min prior to nanoparticle application and throughout the 2-h uptake experiment. The effect of nanoparticles on the uptake of Lucifer yellow (LY), a known fluid-phase marker in hepatocytes and Madin–Darby canine kidney cells (MDCK), was carried out to evaluate if nanoparticles had any stimulatory effect on vesicle formation (endocytosis). First, the kinetics of internalization of 0.1 mM LY in RCEC culture was followed up to 45 min to ensure that it behaves as a fluid-phase tracer. Then, the uptake of LY at the 4-h time period, in the presence and absence of 1 mg/ml nanoparticles, was evaluated. To evaluate the possibility of nanoparticles for enhancing drug delivery to the eye, the uptake at 4-h of a model protein, bovine serum albumin conjugated to Texas-red, TR-BSA, in both free form (0.104 mg/ml) and encapsulated within nanoparticles (1 mg/ml, containing 10.4 w/w of TR-BSA), was examined. Uptake data are presented as mean ± SEM (n), where n is the number of observations. Both Student's *t* test and one-way ANOVA analysis (using Tukey–Kramer test) were used to evaluate significant differences ($p < 0.05$) in sample means, as appropriate.

Nanoparticle Absorption

Semiconfluent RCECs (70–80% confluent on day 5 or 6) were incubated for 2 h at 37°C with a suspension of 6-coumarin nanoparticles (500 μg/ml) and then washed three times with ice-cold BRS buffer to remove excess nanoparticles. This concentration was chosen because it was optimal for distinguishing the fluorescent intensity of nanoparticles from that of the cell autofluorescence. Cells were then fixed with 4% paraformaldehyde solution for 30 min, and the cell filter was mounted on a glass slide using Prolong mounting anti-fade media (Molecular Probes) and viewed under a confocal microscope (Ziess LSM 510, Ziess, Inc., Thornwood, NY) using FITC filter (wavelength, 450–490 nm).

RESULTS

The average transepithelial electrical resistance (TEER) and potential difference (PD) values for RCEC culture (day 7) used in all uptake experiment were 1.20 ± 0.17 kΩ·cm^2 and 3.7 ± 0.75 mV, respectively. Following 2-h incubation with nanoparticles, the TEER and PD values were not significantly different from control ($p > 0.05$) with values of 1.02 ± 0.1 kΩ·cm^2 and 3.1 ± 0.32 mV ($n = 12$), respectively.

In vitro Release of 6-Coumarin

As shown in Fig. 1, 6-coumarin release from nanoparticles followed a biphasic pattern: a rapid initial release that occurred in the first 30 min followed by a slow release afterwards that started to plateau after 8 h. This is a typical release pattern for drugs encapsulated in a matrix system, with the release rate following first-order kinetics. The maximal amount of 6-coumarin released in 24-h was less than 1% (0.32%) of the actual amount of 6-coumarin loaded in the nanoparticles. The contribution of released 6-coumarin (used

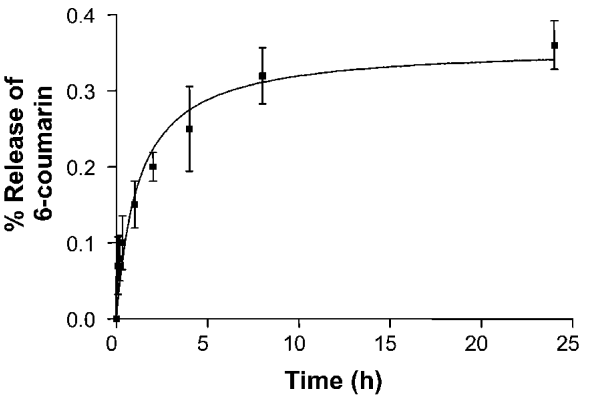

Fig. 1. Percent cumulative *in vitro* release of 6-coumarin from nanoparticles during a 24-h period. Nanoparticles (1 mg/ml) suspended in bicarbonate Ringer's solution (BRS) in a vial were placed on a shaker at 37°C and periodic samples (0.5 ml) were taken and analyzed for coumarin content using a spectrofluorometer. Points represent mean ± SEM ($n = 6$).

as a control) to total nanoparticle uptake did not exceed 10% (data not shown).

Characteristics of Nanoparticle Uptake

As shown in Fig. 2, uptake of nanoparticles reached a plateau after 2 h. Thus, 2-h incubation time was chosen for all further studies. Figure 3 shows that both 100- and 800-nm particles achieved higher uptake values than 10 μm particles. One hundred–nanometer nanoparticles had the highest uptake in primary cultured RCECs, so all further experiments were conducted with these particles. The total uptake of 100-nm nanoparticles increased in a concentration-dependent manner when incubated at 37°C and followed a Michaelis–Menten equation fit (using GraphPad Prism software 3.00, San Diego, CA, USA) with V_{max} of 1.1 ± 0.06 μg/mm^2 and K_m of 0.41 ± 0.07 mg/ml (Fig. 4). Table I indicates that the efficiency of nanoparticle uptake is highest at lower concentration. The amount of nanoparticles transported to the basolateral side amounted to less than 5% of the total uptake (data not shown). Figure 5 demonstrates that uptake of coumarin-loaded PLGA nanoparticles was significantly reduced in a dose-dependent manner by co-incubating RCECs with coumarin-free PLGA nanoparticles of the same size and polymer content.

Lowering the temperature from 37°C to 4°C abolished uptake of PLGA nanoparticles (at three different concentrations) by approximately 90%, indicating that uptake is temperature dependent (Fig. 6). A passive process such as diffusion probably describes the remaining uptake of nanoparticles. The average activation energy (E_a) was 15.3 ± 2.1 kcal/mol determined using Arrhenius analysis of temperature-dependent uptake of the three different nanoparticle concentrations.

Mechanism of Nanoparticle Uptake and Drug Delivery Enhancement

Preincubating nanoparticles for 30 min with either sodium azide or 2,4-dinitrophenol reduced nanoparticle internalization into RCECs by 24 ± 1.5% and 19 ± 0.9%, respectively, compared to that of control (Fig. 7). The internalized fraction of nanoparticles represented 6% of the applied dose of nanoparticles (0.5 mg/ml), whereas the membrane-bound portion was only 1.5%. Figure 7 also demonstrates that the 2-h uptake of 0.5 mg/ml nanoparticles in RCECs decreased significantly when cells were preincubated with 0.1 μg/ml cytochalasin D, an actin filament inhibitor, but not in the presence of 1 μg/ml nocodazole, a microtubule inhibitor, despite a noticeable decrease in uptake pattern.

Table II demonstrates that the uptake of TR-BSA at the 4-h period was 28% higher when given in encapsulated form, as nanoparticles, than when it was applied in free form. We speculated that this increase in protein transport could be mediated by the stimulation of endocytosis (vesicle formation) in RCECs. We tested this by evaluating the effect of

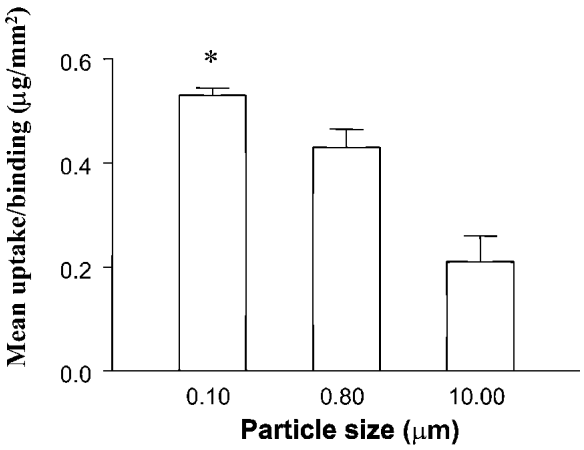

Fig. 3. Effect of size on particle uptake in RCEC culture at 37°C. Different particle sizes (0.1, 0.8, and 10 mm in diameter) were applied to RCEC culture for 2 h. All three different particles were made using PLGA co-polymer and contained both bovine serum albumin (model protein) and 6-coumarin (fluorescent marker). Open bars represent mean ± SEM (n = 6). *Denotes significant differences ($p < 0.05$).

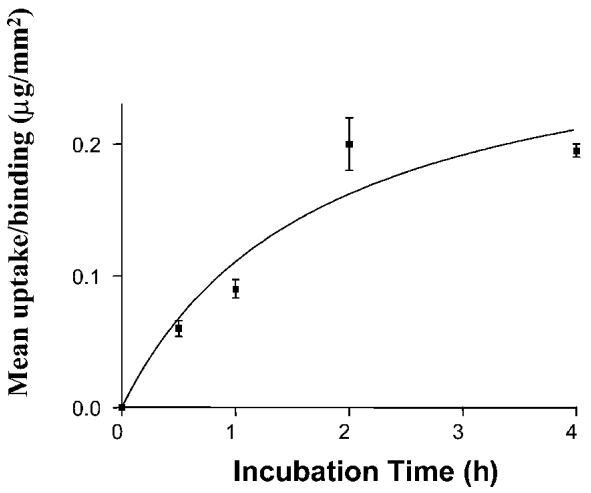

Fig. 2. Effect of incubation time on nanoparticle uptake at 37°C in RCEC culture. The concentration of nanoparticles (100 nm) used was 0.3 mg/ml. K_t represents the time at which half-maximal uptake occurs. The K_t value was 1.74 ± 1.10 h. Symbols (■) represent mean ± SEM (n = 6).

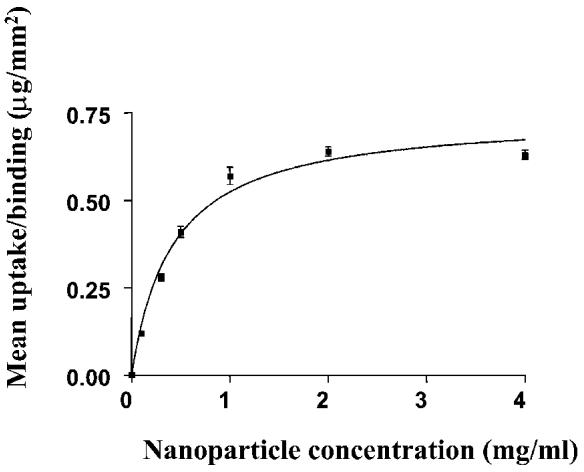

Fig. 4. Effect of concentration on nanoparticle uptake at 37°C in RCEC culture. Various nanoparticle (100 nm) concentrations ranging from 0 to 4 mg/ml were applied to RCEC culture for 2 h Points were fit to a curve using Michaelis–Menten equation. The V_{max} and K_m values were 0.74 ± 0.04 μg/mm^2 and 0.42 ± 0.07 mg/ml, Respectively. Points (■) represent mean ± SEM (n = 6).

Table I. Effect of Nanoparticle Amount on the Number of Particles and Efficiency of Uptake in RCEC Layers

NP Conc (μg/ml)	Amount applied (μg)	Uptake* (μg/mm^2)	Nanoparticles† (No. × 10^9/mm^2)	Efficiency‡ (%)
100	50	0.12 ± 0.011	169.2	24.0
300	150	0.28 ± 0.025	394.8	18.6
500	250	0.41 ± 0.037	578.1	16.4
1000	500	0.57 ± 0.06	803.7	11.4
2000	1000	0.64 ± 0.03	902.4	6.4
4000	2000	0.63 ± 0.033	888.3	3.1

* Values represent mean ± SEM (n = 6).

† No. of particles = [Uptake × k × 10^9]/d^3, where k is a factor that takes into account the density (g/cm^3) of the polymer used and d is the diameter of the particles in μm.

‡ % Efficiency = [Uptake by cells/theoretical dose added] × 100, where theoretical dose is calculated by dividing the total amount of the nanoparticles added by the total area of the RCEC layer exposed to the nanoparticles (100 mm^2).

nanoparticles on the uptake of Lucifer yellow (LY), a fluid-phase marker. Table II shows that simultaneous coadministration of LY with nanoparticles enhanced the uptake of LY at the 4-h period by 39% as compared to LY applied alone. Our observation of the linear uptake of LY over a 60-min period is consistent with it being a fluid-phase marker (data not shown).

Nanoparticle Absorption

Confocal microscopy revealed evidence of nanoparticle uptake, rather than their adsorption to the cell surface. Figure 8a shows that nanoparticles were abundant in the intermediate layer of RCECs just below the apical compartment. Small amounts of nanoparticles were also seen in the deep layer of the cells (not shown). Nanoparticles were seen either distributed in a punctate manner (long arrows) around the cell membrane, in the perinuclear area, below the cell surface, and in distinct compartments (maybe an endosome), or seen in a diffuse pattern (arrowheads) all over the cytoplasm. Nanoparticles were not found in the nuclear region (stained red with propidium iodide). Control images, in the absence of nanoparticles, did not show fluorescence in the cells (Fig. 8b).

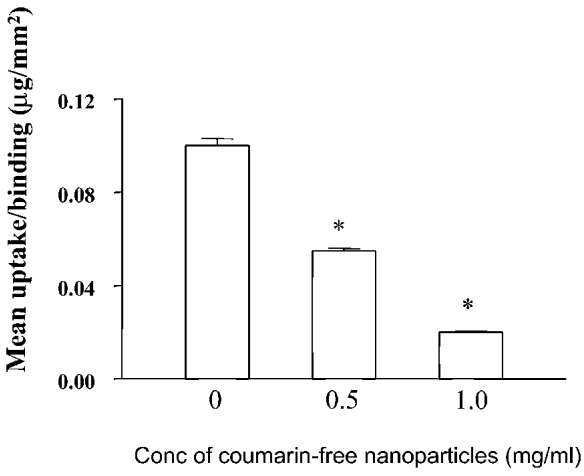

Fig. 5. Effect of inhibition by coumarin-free nanoparticles (competitor) on 6-coumarin nanoparticle uptake at 37°C in RCEC culture. 6-coumarin nanoparticles (0.1 mg/ml) in the presence of different concentrations of unloaded nanoparticles (competitor) at 0, 0.5, and 1 mg/ml were applied to RCEC culture for 2 h. Open bars represent mean ± SEM (n = 6). *Denotes significant differences ($p < 0.05$).

DISCUSSION

Our findings demonstrated that uptake of PLGA particles in rabbit conjunctival epithelial cells is dependent on the particle size, with smaller, 100-nm particles exhibiting the highest uptake compared to larger 800-nm and 10-μm particles. This is consistent with earlier findings by Desai *et al.* (16) showing that Caco-2 cells uptake of PLGA microparticles was time-, size-, and concentration-dependent. Calvo *et al.* (17) observed a similar size-dependency pattern with the *in vivo* corneal uptake of indomethacin-loaded poly(epsilon-caprolactone) colloidal particles being higher than microparticles after topical instillation into the albino rabbit eye.

Confocal microscopy showed that the smaller 100-nm particles were internalized in RCECs rather than adsorbed on the cell surface and were distributed in both a diffused manner in the cytoplasm and in a punctate manner in subcellular, possibly endosomal, compartments. Our studies indicated that 6% of nanoparticle dose (30 μg/cm^2 per 2 h of 0.5 mg/ml) was internalized by conjunctival epithelial cells, and only 1.5% of the dose was surface-bound. The rest of the dose remained in the donor medium. Wood *et al.* (2) observed a lower amount (1% of the dose) in the conjunctival epithelium 6 h postinstillation of poly(hexylcyanoacrylate) nanoparticles *in vivo* into the cul-de-sac area. This could be attributed to the low residence time of the nanoparticles as a result of tear turnover and lacrimal drainage. At the moment, direct comparison of nanoparticle uptake among various epithelial cells is difficult due to differences in the physiochemical properties of nano/microparticulates, animal models, and methods of detection used in different laboratories. Therefore, no conclusion can be drawn regarding the absorption efficiency in these different systems. However, we have studied nanoparticle uptake in Caco-2 cells and have shown that it is comparable to that of RCECs, indicating similar efficiency or mechanism of uptake (data not shown).

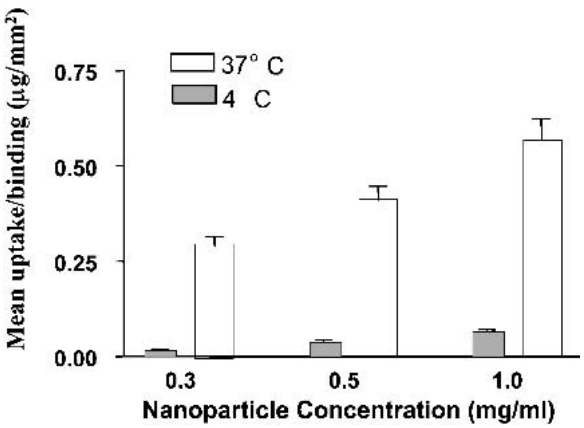

Fig. 6. Effect of temperature on nanoparticle uptake in RCEC culture. Two different temperatures 4°C and 37°C were used to evaluate the uptake of three different concentrations of nanoparticles (0.3, 0.5, and 1 mg/ml, 100-nm particle). Bars represent mean ± SEM (n = 6).

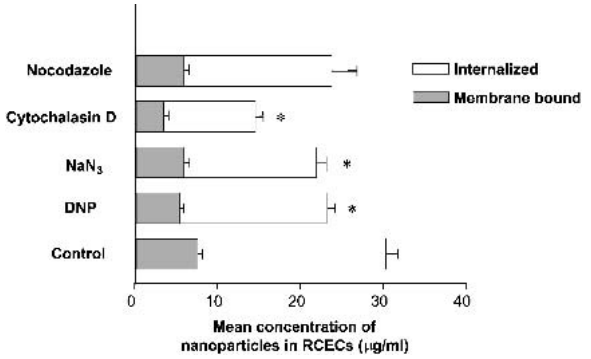

Fig. 7. Effect of energy depletion and vesicle transport inhibitors on nanoparticle uptake in RCEC culture. For energy depletion, RCECs were preincubated with either 10 mM sodium azide or 0.2 mM 2,4-dinitrophenol (metabolic inhibitors) in a glucose-free BRS at 37°C for 30 min prior to 2-h uptake experiment with 0.5 mg/ml nanoparticles. To determine the effects of vesicle transport inhibitors, cells were preincubated at 37°C for 30 min with either 0.1 μg/ml cytochalasin D (actin inhibitor) or 1 μg/ml nocodazole (microtubule inhibitor) before a 2-h nanoparticle uptake study. The membrane-bound fraction was isolated by trypsinization of cells followed by centrifugation (see "Methods"). Bars represent mean ± SEM (n = 4). *Denotes significant differences ($p < 0.05$).

No changes in the potential difference (PD) and transepithelial electrical resistance (TEER) values in RCECs were seen following the 2-h incubation with biodegradable PLGA nanoparticles, which rules out the possible perturbation of tight junctions and ion transport properties by nanoparticles, and supports previous observations of the safety and biocompatability of PLGA polymer following subconjunctival implant in rabbits (18).

We also demonstrated that uptake of 100-nm nanoparticles in RCECs was saturable and inhibited by unloaded-nanoparticles of similar PLGA content and size, implicating the presence of competitive binding sites for the PLGA polymer on the conjunctiva. Lowering the incubation temperature and energy level through the use of metabolic inhibitors reduced nanoparticle uptake in RCECs, which demonstrates that uptake is an active process. Our findings are in concert with previous findings by Pratten and Lloyd (19) demonstrating that uptake of I^{125}-labeled Percoll (consisting of 30-nm silica particles coated with polyvinylpyrrolidone) microparticles in rat visceral yolk sac (VYS) epithelial cell culture was inhibited by low incubation temperature and 2,4-dinitrophenol at the same concentration used (0.2 mM). However, the degree of inhibition of nanoparticle uptake by 2,4-dinitrophenol treatment in our cell system model (19 ± 0.9%) was not as profound as that reported by Pratten and Lloyd (75%). This could be attributed to the higher endocytotic activity (and energy requirement) in visceral yolk sac epithelial cells as part of their nutritional support function to the embryo (20).

At the apical membrane of epithelial cells, vesicle formation for both membrane-bound and fluid-phase markers requires the activity and polymerization of an actin-microfilament network (21), which can be specifically disassembled by cytochalasin D. Treatment of RCECs with cytochalasin D reduced nanoparticle uptake, which indicates that uptake may be occurring by endocytosis. Our cytochalasin inhibition data are in agreement with a previous report for the uptake of nanoparticles by rat glumerular kidney cells (22). Nocodazole, a microtubule inhibitor, did not cause any significant reduction in nanoparticle uptake, which confirmed that microtubules are involved in vesicle transport and not endocytosis or receptor recycling at the plasma membrane. This finding is consistent with the previous report by Pratten and Lloyd (19). The linear uptake pattern of Lucifer yellow over time qualified it as a marker for fluid-phase endocytosis in the conjunctiva (data not shown). This is consistent with previous observation in hepatocytes (23). The significant increase in Lucifer yellow uptake when coadministered with nanoparticles implicates nanoparticles in the induction of endocytosis (vesicle formation). This may explain the mechanism of drug delivery enhancement by nanoparticles, as evidenced by the significant uptake increase of the encapsulated protein (BSA, conjugated to Texas red) at 4-h period. This effect could not be attributed to the protective effect of nanoparticles for BSA (preventing degradation), as we monitored fluorometrically the amount of TR-BSA, rather than BSA alone. A similar enhancement of protein transport across polarized Calu-3 cells (pulmonary epithelial cell line model) using Carbopol gels and chitosan microparticles was previously described (24). In fact our data also confirmed the intracellular stability and sustained-release properties of nanoparticles, as significant amounts of the encapsulated agent were detected 4 days later in RCECs (data not shown).

The uptake behavior of nanoparticles into the kidney (22), the intestine and liver (25), Caco-2 cells (16), and VYS epithelial cells (19) has already been studied. Collectively, these studies explained the uptake mechanisms in terms of both paracellular and transcellular pathways. The tight bar-

Table II. Effect of Nanoparticles on Drug Delivery Enhancement of TR-BSA and on Stimulation of Fluid-Phase Endocytosis of Lucifer Yellow

Chemical used	Total uptake amount ($ng \cdot ml^{-1} \cdot mg^{-1}$mg of protein)	% Relative difference
Texas-red–BSA (as control)	153.0 ± 2.6	Control
Texas-red–BSA-loaded nanoparticles	195.5 ± 9.7*	28% increase in TR-BSA uptake
Lucifer yellow (as control)	119.7 ± 5.5	Control
Lucifer yellow + nanoparticles	166.4 ± 12.9*	39% increase in Lucifer yellow uptake

RCECs were incubated with either 0.104 mg/ml TR-BSA (free form) or 1 mg/ml of TR-BSA–loaded nanoparticles (containing 10.4% w/w of TR-BSA) and incubated at 37°C for 4 h. RCECs were also incubated with 0.1 mM of Lucifer yellow in the absence and presence of 1 mg/ml of nanoparticles at 37°C for 4 h. Values represent mean ± SEM (n = 4).

* Denotes significant differences ($p < 0.05$).

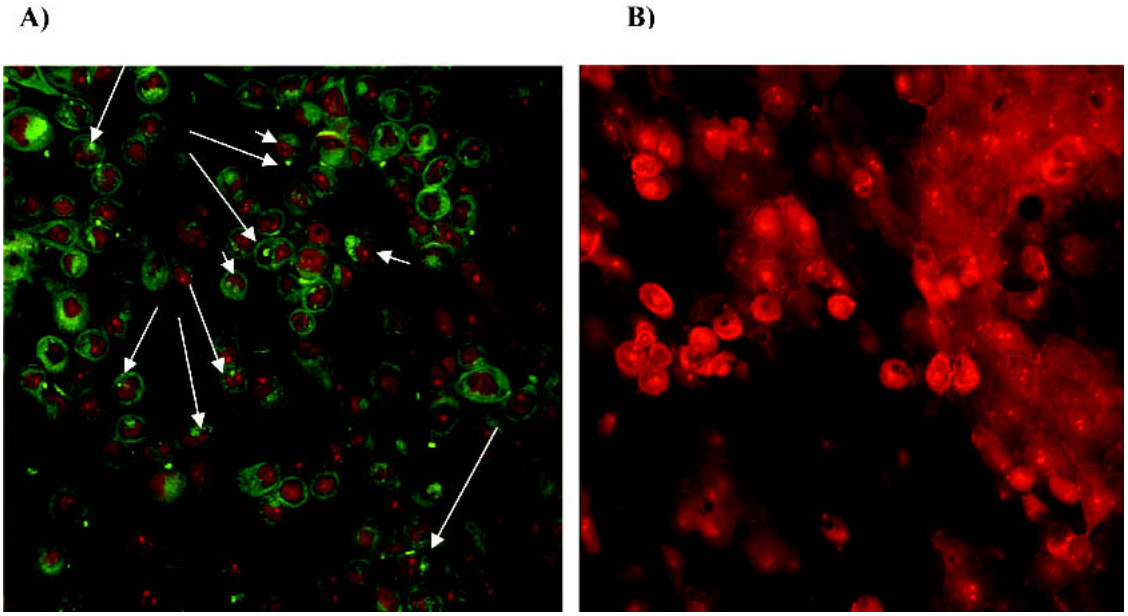

Fig. 8. Confocal microscopy of RCECs after nanoparticles uptake for 2 h. (A) and (B) are X–Y images scanned below the apical plasma membrane (intermediate layer of conjunctival epithelial cells). (A) Represents uptake of nanoparticles by RCECs incubated for 2 h. Nanoparticles are seen within the cytosol, underneath the cell membrane, and in specific compartments (long arrows), but not within the nucleus (small arrows). (B) Control experiment without nanoparticle incubation.

rier properties of the conjunctival epithelium along with the previously estimated paracellular pore radius of 5 nm indicate that nanoparticle uptake occurs mainly by the transcellular pathway (14,26). The uptake of poly(butylcyanoacrylate) nanoparticles into isolated conjunctival epithelial tissues was reported to occur in the first two cell layers only through the transcellular route (4). Our findings support the above assumption. In addition, our findings from the confocal microscopy and the reduction in nanoparticle uptake as a result of energy depletion suggest that endocytosis is the main internalization mechanism of PLGA nanoparticles in RCECs. Ultrastructural evidence for endocytosis (or phagocytosis) of proteins and latex nanospheres (0.8 μm in diameter) in the conjunctival epithelium has previously been reported (27,28). In addition, vesicle formation containing fluorescent nanoparticles in the conjunctival tissue was observed by Zimmer *et al.* (4). All these observations suggest the conjunctival epithelium is capable of endocytosis (or phagocytosis). Because nanoparticle uptake exhibits a saturable pattern and competitive inhibition, fluid-phase endocytosis is not likely to be involved. On the other hand, both adsorptive and receptor-mediated endocytosis involve active and saturable uptake processes, which depend on binding to specific/nonspecific binding sites and receptors, respectively. Because macromolecules transported by the adsorptive pathway have affinity constants in the micromolar range (our K_m is 420 μg/ml) compared to nanomolar range in receptor-mediated endocytosis (29,30), we postulate that nanoparticle uptake in RCECs occur through adsorptive-mediated endocytosis.

CONCLUSIONS

The current study has demonstrated the existence of a nanoparticle uptake process in rabbit conjunctival epithelial cells that is commensurate with adsorptive-mediated endocytosis. The size dependency and efficiency of uptake along with the facilitated uptake of bovine serum albumin indicate that PLGA nanoparticles can be used for the enhancement of drug absorption to the eye and the controlled release of proteins and drugs.

ACKNOWLEDGMENTS

This work was supported by grants from the National Institutes of Health (EY12356, HL38658, HL64365, and HL57234) and the Nebraska Research Initiative-Gene Therapy Program. Some of these data were presented in abstract form at the Association for Research in Vision and Ophthalmology (ARVO 2001) scientific meeting [M. Q. Qaddoumi *et al.* The mechanism of uptake of biodegradable PLGA nanoparticles in conjunctival epithelial cell layers. IOVS **42**(4):S501 (2001)].

REFERENCES

1. C. L. Bourlais, L. Acar, H. Zia, P. A. Sado, T. Needham, and R. Leverge. Ophthalmic drug delivery systems—recent advances. *Prog. Retin. Eye Res.* **17**:33–58 (1998).
2. R. Wood, V. Li, J. Kreuter, and J. Robinson. Ocular disposition of poly-hexyl-2-cyano [3-^{14}C] acrylate nanoparticles in the albino rabbit. *Int. J. Pharm.* **23**:175–183 (1985).
3. A. Zimmer, P. Chetoni, M. Saettone, and H. Zerbe, and J. Kreuter. Evaluation of pilocarpine-loaded albumin nanoparticles as controlled drug delivery systems for the eye. II co-administration with bioadhesive and viscous polymers. *J. Controll. Rel.* **33**: 31–46 (1995).
4. A. Zimmer, J. Kreuter, and J. R. Robinson. Studies on the transport pathway of PBCA nanoparticles in ocular tissues. *J. Microencapsul.* **8**:497–504 (1991).
5. L. Marchal-Heussler, D. Sirbat, M. Hoffman, and P. Maincent. Poly(epsilon-caprolactone) nanocapsules in carteolol ophthalmic delivery. *Pharm. Res.* **10**:386–390 (1993).
6. M. Hashizoe, Y. Ogura, T. Takanashi, N. Kunou, Y. Honda, and

Y. Ikada. Biodegradable polymeric device for sustained intravitreal release of ganciclovir in rabbits. *Curr. Eye Res.* **16**:633–639 (1997).
7. R. Diepold, J. Kreuter, J. Himber, R. Gurny, V. H. Lee, J. R. Robinson, M. F. Saettone, and O. E. Schnaudigel. Comparison of different models for the testing of pilocarpine eyedrops using conventional eyedrops and a novel depot formulation (nanoparticles). *Graefes Arch. Clin. Exp. Ophthalmol.* **227**:188–193 (1989).
8. D. K. Gilding and A. M. Reed. Biodegradable polymers for use in surgery: poly(glycolic) / poly(lactic acid) homo- and copolymers. *Polymer* **20**:1459–1464 (1979).
9. P. N. Dilly. Contribution of the epithelium to the stability of the tear film. *Trans. Ophthalmol. Soc. U. K.* **104**:381–389 (1985).
10. K. M. Hamalainen, K. Kananen, S. Auriola, K. Kontturi, and A. Urtti. Characterization of paracellular and aqueous penetration routes in cornea, conjunctiva, and sclera. *Invest. Ophthalmol. Vis. Sci.* **38**:627–634 (1997).
11. P. Saha, T. Uchiyama, K. J. Kim, and V. H. Lee. Permeability characteristics of primary cultured rabbit conjunctival epithelial cells to low molecular weight drugs. *Curr. Eye Res.* **15**:1170–1174 (1996).
12. J. Davda and V. Labhasetwar. Characterization of nanoparticle uptake by endothelial cells. *Int. J. Pharm.* **233**:51–59 (2002).
13. U. B. Kompella, K. J. Kim, and V. H. Lee. Active chloride transport in the pigmented rabbit conjunctiva. *Curr. Eye Res.* **12**:1041–1048 (1993).
14. P. Saha, K. J. Kim, and V. H. Lee. A primary culture model of rabbit conjunctival epithelial cells exhibiting tight barrier properties. *Curr. Eye Res.* **15**:1163–1169 (1996).
15. J. J. Yang, H. Ueda, K. Kim, and V. H. Lee. Meeting future challenges in topical ocular drug delivery: development of an air-interfaced primary culture of rabbit conjunctival epithelial cells on a permeable support for drug transport studies. *J Controll. Rel.* **65**:1–11 (2000).
16. M. P. Desai, V. Labhasetwar, E. Walter, R. J. Levy, and G. L. Amidon. The mechanism of uptake of biodegradable microparticles in Caco-2 cells is size dependent. *Pharm. Res.* **14**:1568–1573 (1997).
17. P. Calvo, M. J. Alonso, J. L. Vila-Jato, and J. R. Robinson. Improved ocular bioavailability of indomethacin by novel ocular drug carriers. *J. Pharm. Pharmacol.* **48**:1147–1152 (1996).
18. G. Wang, I. G. Tucker, M. S. Roberts, and L. W. Hirst. In vitro and in vivo evaluation in rabbits of a controlled release 5-fluorouracil subconjunctival implant based on poly(D,L-lactide-co-glycolide). *Pharm. Res.* **13**:1059–1064 (1996).
19. M. K. Pratten and J. B. Lloyd. Uptake of microparticles by rat visceral yolk sac. *Placenta* **18**:547–552 (1997).
20. W. P. Jollie. Ultrastructural studies of protein transfer across rodent yolk sac. *Placenta* **7**:263–281 (1986).
21. T. A. Gottlieb, I. E. Ivanov, M. Adesnik, and D. D. Sabatini. Actin microfilaments play a critical role in endocytosis at the apical but not the basolateral surface of polarized epithelial cells. *J. Cell Biol.* **120**:695–710 (1993).
22. L. Manil, J. C. Davin, C. Duchenne, C. Kubiak, J. Foidart, P. Couvreur, and P. Mahieu. Uptake of nanoparticles by rat glomerular mesangial cells in vivo and in vitro. *Pharm. Res.* **11**:1160–1165 (1994).
23. J. A. Oka, M. D. Christensen, and P. H. Weigel. Hyperosmolarity inhibits galactosyl receptor-mediated but not fluid phase endocytosis in isolated rat hepatocytes. *J. Biol. Chem.* **264**:12016–12024 (1989).
24. C. Witschi and R. J. Mrsny. In vitro evaluation of microparticles and polymer gels for use as nasal platforms for protein delivery. *Pharm. Res.* **16**:382–390 (1999).
25. E. Sander and C. Ashworth. A study of particulate intestinal absorption and hepatocellular uptake. *Exp. Cell Res.* **22**:137–145 (1961).
26. Y. Horibe, K. Hosoya, K. J. Kim, T. Ogiso, and V. H. Lee. Polar solute transport across the pigmented rabbit conjunctiva: size dependence and the influence of 8-bromo cyclic adenosine monophosphate. *Pharm. Res.* **14**:1246–1251 (1997).
27. P. Steuhl and J. W. Rohen. Absorption of horseradish peroxidase by the conjunctival epithelium of monkeys and rabbits 1. *Graefes Arch. Clin. Exp. Ophthalmol.* **220**:13–18 (1983).
28. S. Latkovic and S. E. Nilsson. Phagocytosis of latex microspheres by the epithelial cells of the guinea pig conjunctiva. *Acta Ophthalmol. (Copenh.)* **57**:582–590 (1979).
29. J. L. Goldstein, M. S. Brown, R. G. Anderson, D. W. Russell, and W. J. Schneider. Receptor-mediated endocytosis: concepts emerging from the LDL receptor system. *Annu. Rev. Cell Biol.* **1**:1–39 (1985).
30. Y. Sai, M. Kajita, I. Tamai, J. Wakama, T. Wakamiya, and A. Tsuji. Adsorptive-mediated endocytosis of a basic peptide in enterocyte-like Caco-2 cells. *Am. J. Physiol.* **275**:G514–G520 (1998).